Achieving Specificity in Selected and Wild-Type N Peptide−RNA Complexes: The Importance of Discrimination against Noncognate RNA Targets[†]

Jeffrey E. Barrick[‡] and Richard W. Roberts*

Division of Chemistry and Chemical Engineering, California Institute of Technology, Pasadena, California 91125

Received July 7, 2003; Revised Manuscript Received August 13, 2003

ABSTRACT: The boxB RNA pentaloops from the P22 and λ phages each adopt a GNRA tetraloop fold upon binding their cognate arginine-rich N peptides. The third loop base in P22 boxB (3-out) and the fourth in λ boxB (4-out) are excluded to accommodate this structure. Previously, we selected a pool of λ N sequences with random amino acids at loop contacting positions 13−22 for binding to either of these two GNRA-folded pentaloops or a canonical GNRA tetraloop and isolated a class of peptides with a new conserved arginine (R15). Here, we characterize the binding of λ N and these R15 peptides using fluorescent titrations with 2-aminopurine labeled versions of the three GNRA-folded loops and circular dichroism spectrometry. All peptides preferentially bind the λ boxB RNA loop. λ N and R15 peptide specificity against the P22 loop arises from the cost of rearranging its loop into the 4-out GNRA structure. Modeling indicates that the interaction of R8 with an additional loop phosphate in the 4-out GNRA pentaloop selectively stabilizes this complex relative to the tetraloop. R15 peptides gain additional discrimination against the tetraloop because their arginine also preferentially interacts with the 4-out GNRA pentaloop phosphate backbone, whereas K14 and W18 of λ N contribute equal affinity when binding the tetraloop. Nonspecific electrostatic interactions by basic residues near the C-termini of these peptides create significantly steeper salt dependencies in association constants for noncognate loops, aiding discrimination at high salt concentrations. Our results emphasize the importance of considering specificity against noncognate as well as nonspecific targets in the combinatorial and rational design of biopolymers capable of macromolecular recognition.

Short terminal extensions of several viral proteins involved in transcriptional regulation exhibit high binding specificity and affinity for RNA folds as isolated peptides (*1, 2*). Unlike RNA-binding protein domains, these arginine-rich peptides are unstructured in solution and only adopt α helix or β strand secondary structure upon binding their RNA targets. Peptide binding causes less dramatic reciprocal changes in RNA structure: inducing base flips, stabilizing nonstandard base pairs, and widening the binding groove. For example, the HIV Rev arginine-rich peptide recognizes both a natural cognate RRE[1] RNA site and an RNA aptamer isolated by in vitro selection with high affinity and specificity (*3*). The Rev peptide assumes a condensed helical structure when bound to RRE and a completely different extended conformation when bound to the aptamer. It is difficult to predict and design arginine-rich peptide specificity against different RNA targets because of this reciprocal induced fit. The homologous N peptides from phages λ and P22 offer a unique opportunity for comparing arginine-rich peptide specificity

because they recognize GNRA-folded RNA loops differing by a single nucleotide.

GNRA tetraloops (N = A, T, C, G; R = A, G) are the most common hairpin motif in ribosomal RNA and are widespread in other functional RNAs. They fold into a stable, compact structure where the closing bases form a sheared G:A pair and the purine base at the third loop position stacks on the 3′ side of the loop. Specific hydrogen bonds stabilize this conformation: the G amine hydrogen bonds to the R3pA4 phosphate on the opposite strand, and the purine at position 3 hydrogen bonds to the 2′ OH of G1 (*4−6*). Larger loops can adopt functional GNRA tetraloop structures. A GAAA loop that interacts with the GNRA tetraloop receptor of the group II intron can be replaced with a GAAAA pentaloop with almost no loss of function, and even six nucleotide loops that maintain a GN$_n$RA consensus are active (*7*).

The solution structures of the λ and P22 N peptides bound to their boxB RNA binding sites have been solved by NMR (*8−10*). In complex with the cognate N peptides, four nucleotides of the GAAAA λ boxB and GACAA P22 boxB RNA pentaloops adopt a canonical GNRA tetraloop fold by flipping out the remaining base (Figure 1). In the λ N-boxB complex (Figures 1 and 2), tetraloop folding excludes A4 and packs it against the A3 sugar away from the major groove (*8, 9*). In the P22 N-boxB complex, tetraloop folding excludes C3 to protrude along the major groove side of the hairpin where it contacts the bound peptide (*10*). We refer

* To whom correspondence should be addressed. E-mail: rroberts@caltech.edu.

‡ Present address: Department of Molecular Biophysics and Biochemistry, Yale University, P. O. Box 208114, New Haven, CT 06520.

[1] Abbreviations: RRE, Rev response element; 2AP, 2′-methoxy, 2-aminopurine; SK_{obs}, salt dependence; CD, circular dichroism.
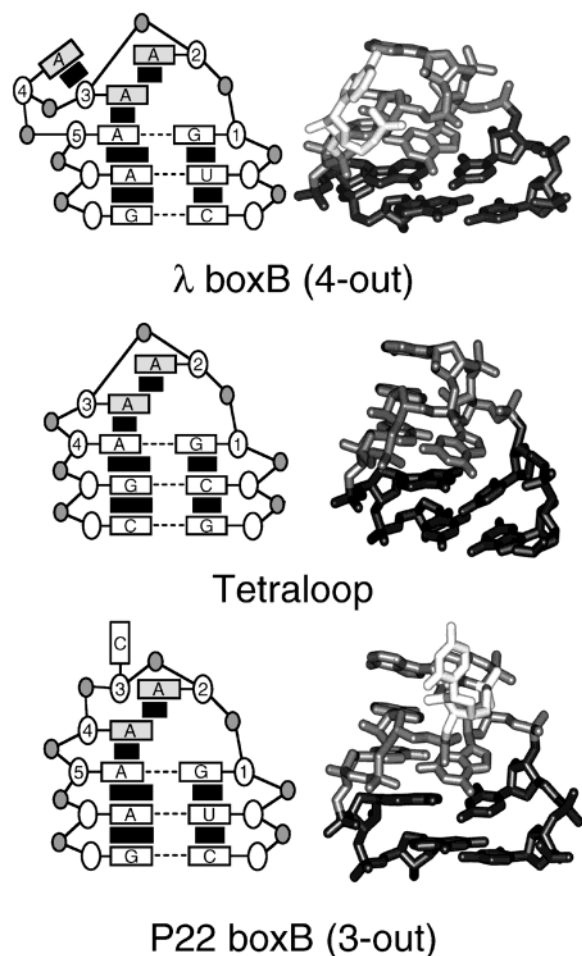
λ boxB (4-out)

Tetraloop

P22 boxB (3-out)

FIGURE 1: Schematics and structures of the GNRA-folded loops examined. The schematics show the different stacking patterns of the loop nucleotides in the λ boxB (*8*) and P22 boxB (*10*) pentaloops as compared to the GAAA tetraloop (*5*). The representations shown here were adapted from these individual references. The RNA base, ribose, and phosphate groups are depicted as rectangles, ovals, and gray circles, respectively. Black rectangles represent stacking interactions, and dashed lines show base pairing. Bases shaded gray were individually substituted with the fluorescent probe 2′-methoxy-2-aminopurine for our binding studies. The structures of λ boxB, tetraloop, and P22 boxB are 1QFQ, 1ZIF, and 1A4T from the Protein Data Bank. The four nucleotides forming the GNRA turn are gray, the extruded loop nucleotide in λ BoxB and P22 BoxB is white, and the base-paired stem is black. For λ BoxB and P22 BoxB, the RNA loop structures were determined in complex with their cognate N peptides. The tetraloop and P22 boxB loop sequences were grafted onto the λ boxB base-paired stem for our binding studies to eliminate unnecessary variation between RNA targets.

to these idealized conformations as 4- and 3-out GNRA pentaloops to denote which loop nucleotide is excluded from the tetraloop fold. These two ways of achieving a GNRA fold within a pentaloop present more varied backbone conformations and hydrophobic surfaces for peptide recognition than a canonical GNRA tetraloop.

The presence of favorable electrostatics, hydrogen bonding, and hydrophobic packing in the structure of an N peptide-boxB RNA complex provides a detailed description of where high affinity binding for that boxB RNA target originates. However, cognate structures do not give any insight into which contacts confer specificity against binding other RNA structures. The in vivo antitermination activities of many mutant λ boxB sequences (*11*) and λ N peptides
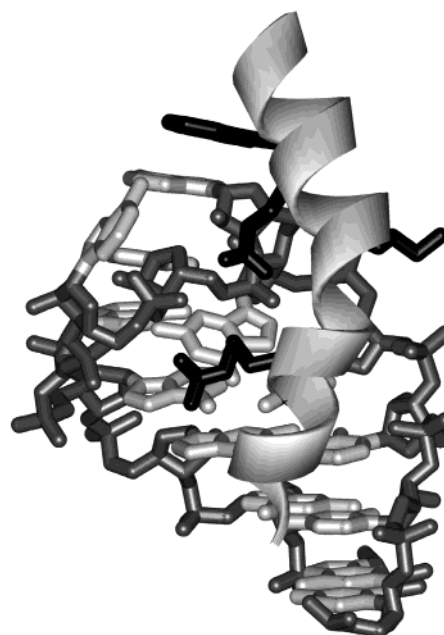

FIGURE 2: Structure of the λ N peptide-boxB RNA complex. The λ boxB RNA is shown as a stick model with the nitrogenous bases in light gray and the sugar phosphate backbone in dark gray. The bound λ N peptide (1−22) is shown as a ribbon with the R8, K14, Q15, and W18 side chains discussed in the text shown as black stick models.

(*12*) as well as chimeras of N peptides from different species (*13*) have been determined by assaying viral viability or following reporter constructs. The affinities of mutant N peptides and boxB RNAs have been directly measured in vitro by gel mobility shift (*13*−*15*), native tryptophan fluorescence quenching (*16*), and gel coelectrophoresis (*17*). Additionally, different conformational changes upon binding in several mutant complexes have been noted by circular dichroism (*9*, *14*−*16*). Even with this extensive biophysical characterization of N peptides, there is more to learn about the structural basis for λ N and P22 N peptide binding specificity. Whether these mutant association constant differences are the consequences of changes in RNA or peptide folding or altered intermolecular interactions in noncognate complexes has not been examined in detail.

We were interested in the degree to which changing the loop interacting sequence of an N peptide could influence its specificity among different GNRA-folded loops. To this end, we used mRNA display to exhaustively search a pool of 9×10^{12} individual peptide sequences based on λ N (*1*−*22*) where the codons at positions 13−22 were randomized to encode any amino acid. We isolated sequences that bound to an equimolar mixture of three immobilized GNRA-folded loops in the presence of nonspecific tRNA competitor (*18*). The targets all had the stem sequence of λ boxB with different loop sequences: a GAAA tetraloop, the λ boxB GAAAA pentaloop, and the P22 boxB GACAA pentaloop (Figure 1). After 12 rounds of selection, peptides with a conserved arginine at position 15 dominated the pool population. Steady state fluorescence titrations with 2-aminopurine (2AP) substituted RNA targets showed that all of these peptides preferentially recognize the λ boxB loop. We subsequently used circular dichroism spectrometry to verify sequence analysis predictions that selected peptide random regions continue the bent α helix of the λ N stem up to

position 17 on average in cognate λ boxB complexes (*19*). We have continued the biophysical characterization of wild-type λ N and selected peptides (Figure 3) here by (1) varying the monovalent cation concentration during titrations to determine the salt dependence of peptide discrimination among the three RNA targets, (2) substituting each loop adenine in all three targets individually with 2AP to characterize RNA loop conformational changes induced by peptide binding from fluorescence changes, and (3) measuring the helicity of peptides bound to all three RNA targets to determine peptide conformational changes induced by RNA binding. On the basis of these results, we propose a model that explains the different specificities of λ N and R15 peptides.

MATERIALS AND METHODS

Fluorescence Titrations. RNA targets substituted with 2′-methoxy, 2-aminopurine (2AP) were chemically synthesized and gel purified. The λ boxB base-paired stem flanked each RNA target's loop sequence (5′-GGCCCU-[loop]-AGGGCC). Peptides with free acid and amine termini were synthesized by standard Fmoc or Boc solid-phase chemistries and purified by reverse-phase HPLC. In a titration experiment, concentrated peptide was added stepwise to a stirred solution of 20−500 nM RNA target at 20 °C. The intensity of 2AP fluorescence was monitored at a wavelength of 370 nm after excitation at 310 nm. For most peptides, binding buffer was 20 mM Tris·OAc supplemented with KOAc to achieve different monovalent cation concentrations and readjusted to pH 7.5 with additional HOAc. Because of its weak binding affinity, λ N (1−11) titrations were conducted in 2−20 mM Tris·OAc (pH 7.5). All pH values were measured at room temperature (25 °C).

Binding constants were determined from fluorescence titration curves (F_T) by least-squares fitting to a single site association model (eq 1). [P], [R], and [C] represent the equilibrium concentrations of peptide, RNA target, and peptide−RNA complex, respectively. $[P]_0$ and $[R]_0$ are the initial concentrations of peptide and RNA target added to the solution. The association constant (K_{obs}), free RNA fluorescence (F_R), and peptide−RNA complex fluorescence (F_C) were fit as free parameters for all titrations. Free peptide fluorescence (F_P) was set to zero for all peptides except λ N (1−22) and 11−10 where it was fit as an additional free parameter. The fluorescence from native tryptophan residues in these peptides produces an interfering signal that is 30−50 times less intense than 2AP at our excitation and emission wavelengths.

$$F_T = ([P]_0 - [C])F_P + ([R]_0 - [C])F_R + [C]F_C$$

$$[C] = \frac{1}{2}([P]_0 + [R]_0 + K_{obs}^{-1} - \sqrt{[P]_0 + [R]_0 + K_{obs}^{-1} - 4[P]_0[R]_0}) (1)$$

Salt dependencies ($\Delta n = SK_{obs}$) for peptide−RNA binding were determined by least-squares fitting of the association constants determined from individual titrations at different salt concentrations to eq 2. $[M^+]$ is the total monovalent cation concentration equal to [Tris] + [K⁺], and K_{1M} is

the association constant at the standard condition where $[M^+] = 1$ M.

$$K_{obs} = K_{1M}[M^+]^{-\Delta n} \qquad (2)$$

Fluorescence changes caused by peptide binding were recorded as the ratio of F_C to F_R. The structure of free RNA targets varies with the monovalent cation concentration. Consequently, F_R for individual titrations was corrected to a standard condition of 20 mM Tris·OAc (pH 7.5) using a reference curve constructed by titrating KOAc into a solution of 2AP RNA in 20 mM Tris·OAc (Supporting Information). The structures of RNA−peptide complexes appear to be largely independent of $[M^+]$, so F_C was not corrected. The titration of additional KOAc above a concentration of 600 mM causes the fluorescence of all seven 2AP labeled RNA targets to decrease. We interpret this uniform quenching as an aggregation of RNA hairpins into base-paired dimers and higher order structures. All peptide titrations used to determine salt dependencies were conducted at or below this monovalent cation concentration to ensure monomeric RNA targets.

Circular Dichroism Spectra. Complexed peptide difference spectra were determined and analyzed as previously described (*19*). The RNA targets used for these measurements had shorter 5 nt base-paired stems (5′-GCCCU-[loop]-AGGGC). Free RNA spectra at high magnesium concentration were determined in a low phosphate buffer (0.1 mM potassium phosphate; 10 mM KCl; 200 mM MgCl₂; pH 7.3) to avoid Mg₃(PO₄)₂ precipitation.

Structural Modeling. The structures of the GAAA tetraloop (*6*), λ N-boxB complex (*9*), and P22 N-boxB complex (*10*) were retrieved as entries 1ZIF, 1QFQ, and 1A4T from the Protein Data Bank. These structures have the exact loop sequences of the targets examined here but different sequences in the base-paired stems. To compare the positions of λ N residues with respect to noncognate hairpins, the three structures were aligned using the backbone atoms of the loop G:A pair and the two adjacent base pairs of each stem in SwissPdbViewer (*20*).

RESULTS

λ boxB Binding. We used the changes in fluorescence of 2′-methoxy, 2-aminopurine (2AP) substituted RNA loops induced by N peptide binding to measure RNA−peptide association constants (Figure 4). To compare peptide specificities over a wide range of buffer conditions, we determined binding constants to RNA targets labeled at the second loop position (2AP-2) at different monovalent salt concentrations (Figure 5). One can also deduce the relative importance of

```
             1 2 3 4 5 6 7  8 9 10 11 12 13 14 15 16 17 18 19 20 21 22
λ N (1-11)   M D A Q T R R R E R R G Y
λ N (1-22)   - - - - - - - - - - - A E K Q A Q W K A A N
11-10        - - - - - - - - - - - A L R N E K F W V V
11-36        - - - - - - - - - - - M E R A T L P Q V L
12-39        - - - - - - - - - - - L Q R S R A R H A L
12-47        - - - - - - - - - - - L E R T K L E K A L
12-50        - - - - - - - - - - - N M R M Y R S L V I
```

FIGURE 3: Sequences of wild-type λ N peptide and in vitro selected R15 peptides used in this study. A dash (−) denotes that an amino acid is the same as in the preceding row. The 11 N terminal amino acids are conserved in all selected peptides. Peptide designations are the round of selection that they were sequenced in followed by a clone number.
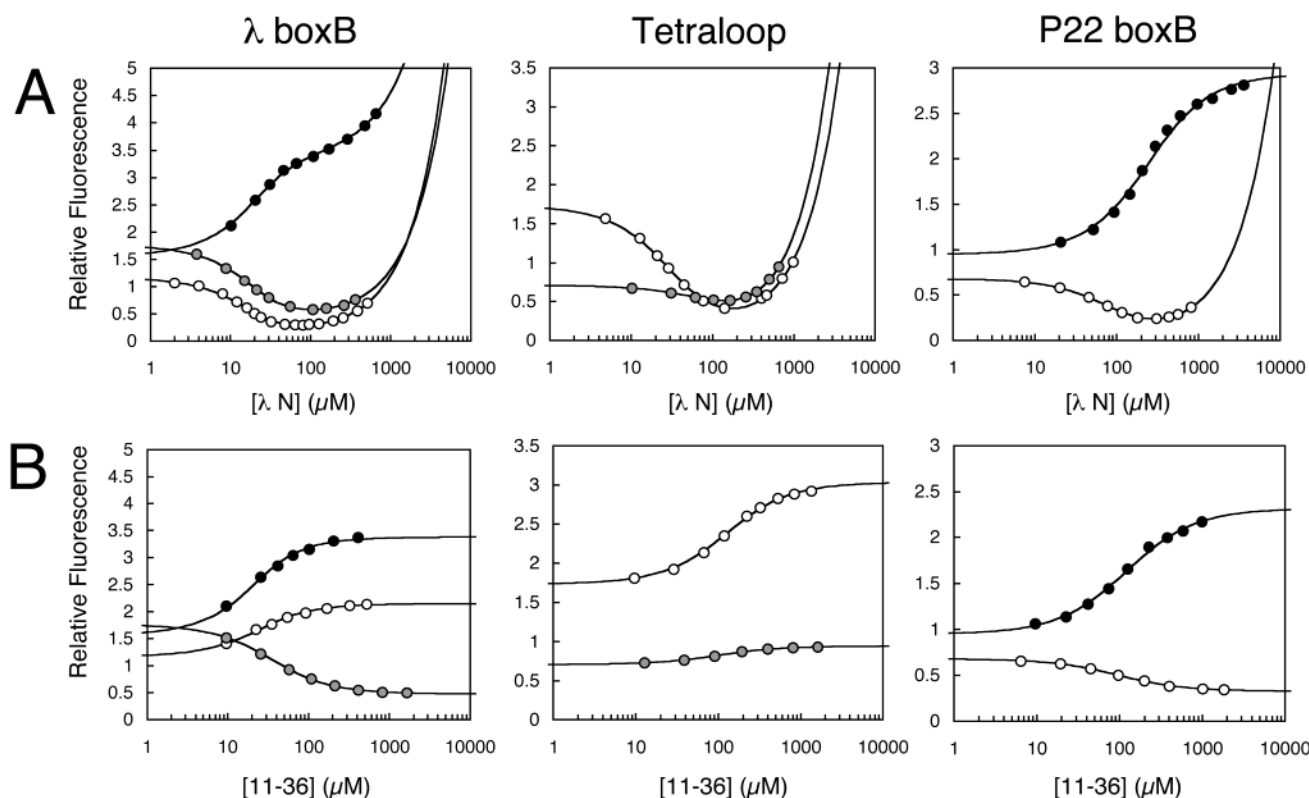
FIGURE 4: Fluorescent titrations with 2-aminopurine labeled RNA loops. Different RNA target and monovalent cation concentrations added to the standard 20 mM Tris·Cl buffer were necessary to maintain binding constants in a range that could be accurately measured. (A) Wild-type λ N (1−22) to λ boxB (20 nM RNA; 100 mM K^+), tetraloop (20 nM RNA; 75 mM K^+), and P22 boxB (2AP-2: 60 nM RNA and 2AP-4: 120 nM; 50 mM K^+). (B) Peptide 11−36 to λ boxB (20 nM RNA; 100 mM K^+), tetraloop (60 nM RNA; 25 mM K^+), and P22 boxB (20 nM RNA; 25 mM K^+). Experimental values are shown as circles shaded to represent the position of 2AP labeling in the titration: 2AP-2 (white), 2AP-3 (gray), and 2AP-4 (black). All fluorescence values are relative to free λ boxB 2AP-2 in 20 mM Tris·Cl buffer. The lines represent least-squares fits where the K_{obs}, free RNA signal, and RNA−peptide complex signal were free parameters. In panel A, interfering fluorescence from the native tryptophan in λ N (1−22) causes the signal to increase at high peptide concentrations near the titration endpoints. Free peptide signal was included as an additional free parameter for these fits.

electrostatic contacts in each RNA−peptide complex from the salt dependence of its association constant.

Increasing the monovalent salt concentration typically weakens the association of a positively charged ligand and nucleic acid. This effect can be thermodynamically formulated as a binding equilibrium including Δn, the effective number of monovalent cations released from the nucleic acid (N) upon polycationic ligand (L) binding (eq 3).

$$[N] + [L] \rightleftharpoons [NL] + \Delta n[M^+] \qquad (3)$$

Assuming each positive charge in the ligand substitutes for bound cations at one phosphate and making appropriate approximations (21) allows one to calculate Δn and the dependence of K_{obs} on the salt concentration (eq 4).

$$-\frac{\partial \log K_{obs}}{\partial \log [M^+]} = Z\psi = SK_{obs} \qquad (4)$$

SK_{obs} is referred to as the salt dependence of the binding interaction. Z is the total number of ligand positive charges. ψ is the net number of thermodynamically associated monovalent cations per nucleic acid phosphate from counterion condensation and electrostatic screening. ψ values for double-stranded RNA and double- and single-stranded DNA are 0.90, 0.88, and 0.70, respectively. Measurements of SK_{obs} for short oligolysines and oligoarginines with a single tryptophan binding nonspecifically to DNA and RNA ho-

mopolymers agree well with the values calculated from their net charges (22, 23). This model also predicts the salt dependence of model alanine-based peptides containing spaced lysines binding to calf thymus DNA (24). Nucleic acid binding increases the amount of helical secondary structure present in these peptides, reminiscent of N peptide binding.

However, specific binding of folded proteins to particular nucleic acid sites typically has a much smaller salt dependence than these models predict. In these cases, the individual contribution of each charged side chain to SK_{obs} depends on its local environment in the defined macromolecular structure. The best-studied complex is the interaction of ribosomal protein L11 with its rRNA binding site (25). The side chain contributions of its arginine and lysine residues to SK_{obs} determined by site-specific mutagenesis range from −0.07 to +0.74, and double mutants exhibit substantial nonadditivity. Calculating the salt dependence of specific protein binding to a nucleic acid requires known molecular structures and finite difference solutions to the nonlinear Poisson−Boltzmann equation (26) or Monte Carlo simulations (27).

Wild-type λ N (1−22) peptide has an SK_{obs} value of 2.5 for binding λ boxB (Table 1). Eq 1 predicts a salt dependence of 3.6 for λ N (1−22) binding nonspecifically to λ boxB from its net +4 charge and approximating the hairpin as double-stranded RNA ($\psi = 0.90$). The salt dependence could theoretically be as high as 6.3 if the seven positively charged
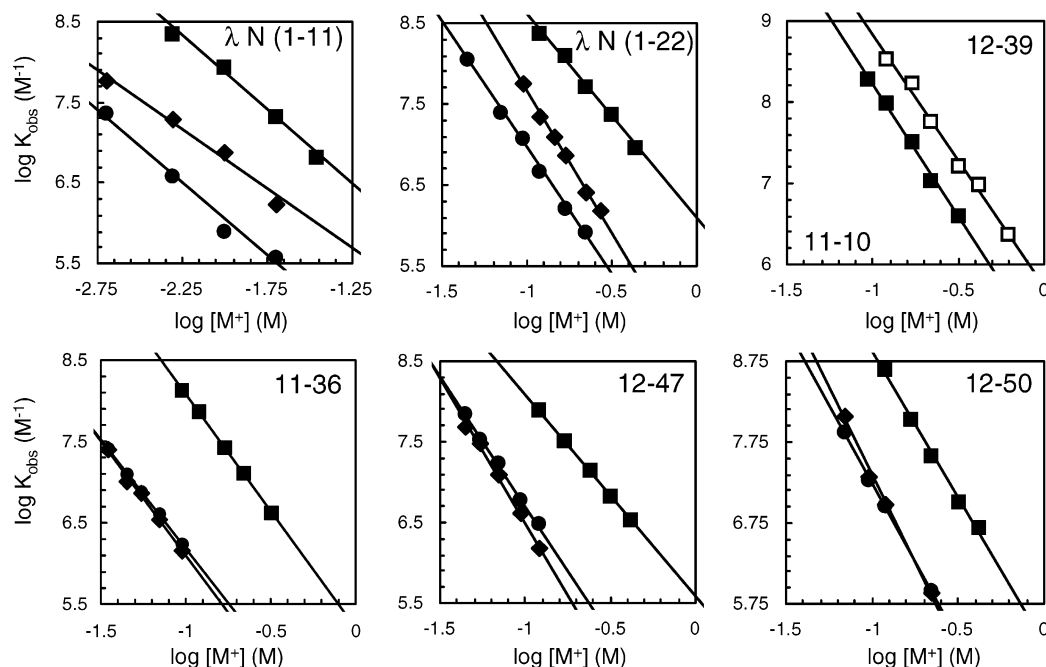
FIGURE 5: Salt dependence of peptide binding to target RNAs. Multiple titrations with λ boxB 2AP-2 (squares), tetraloop 2AP-2 (diamonds), and P22 boxB 2AP-2 (circles) at different concentrations of monovalent cation were used to determine $\partial \log K / \partial \log [M^+]$ values. $[M^+]$ is the total monovalent cation concentration. Titrations for λ N (1−11) at $[M^+] < 20$ mM used a Tris·OAc buffer with $[M^+] = [Tris]$. All other titrations at $[M^+] > 20$ mM used a constant 20 mM Tris·OAc buffer supplemented with KOAc such that $[M^+] = [Tris] + [K^+]$. Lines are least-squares fits to the exponential form of the salt dependence equation. In the upper right graph, data for two peptides are shown with 12−39 in white and 11−10 in black.

Table 1: Salt Dependencies of RNA−Peptide Association Constants[a]

	λ boxB 2AP−2		tetraloop 2AP−2		P22 boxB 2AP−2	
	SK_{obs}	K_{1M}	SK_{obs}	K_{1M}	SK_{obs}	K_{1M}
λ N (1−11)	1.8 ± 0.1	15 ± 9	1.5 ± 0.2	7 ± 6	1.8 ± 0.1	0.3 ± 0.2
λ N (1−22)	2.5 ± 0.1	1200 ± 200	3.50 ± 0.08	14 ± 2	3.12 ± 0.08	7 ± 1
11−10	3.3 ± 0.1	90 ± 20	−	−	−	−
11−36	2.87 ± 0.04	160 ± 10	2.8 ± 0.1	2.0 ± 0.7	2.67 ± 0.03	3.2 ± 0.3
12−39	3.1 ± 0.2	600 ± 100	−	−	−	−
12−47	2.56 ± 0.02	390 ± 10	3.6 ± 0.2	0.9 ± 0.4	3.19 ± 0.06	3.4 ± 0.5
12−50	3.6 ± 0.1	180 ± 40	4.3 ± 0.2	1.0 ± 0.5	3.9 ± 0.01	2.3 ± 0.6

[a] K_{1M} is the intercept (in mM^{-1}), and $SK_{obs} = -\delta \log K_{obs}/\delta \log [M^+]$ is the negative of the slope of the salt dependence curves. A dash indicates that a value was not measured.

side chains could localize near the RNA while the three negatively charged side chains remained distant. Therefore, the measured salt dependence agrees with the known specific structure of the peptide−RNA complex wherein the contributions of individual positively charged side chains to SK_{obs} are smaller and depend on their structural context. To directly compare the effects of the different C-terminal residues at positions 13−22 in selected peptides to λ N (1−22), we measured the salt dependence of the constant 11 amino acid N-terminal fragment of λ N that includes its arginine-rich region. λ N (1−11) has a low SK_{obs} value of 1.8 and has been previously shown to discriminate against binding noncognate P22 and GAAA loop sequences as well as the full-length λ N peptide (*18*). Since this N-terminal fragment apparently retains the same specific RNA-bound structure as it does within λ N (1−22), the increase in salt dependence from 1.8 to 2.5 is an additive effect of interactions with residues 13−22.

The full nonlinear Poisson−Boltzmann calculations of salt dependence for protein binding reflect ion reorganization contributions from (1) replacement of nucleic acid localized

cations by basic side chains, (2) secondary stabilization of localized cations by acidic side chains, and (3) solvent and cation exclusion from the volume near the nucleic acid by the bound peptide. Each of these effects will be strongest in the vicinity of the RNA phosphate backbone where cations are initially concentrated. K14 and Q15 are the only side chains from positions 13−22 of λ N able to contact the λ boxB RNA backbone in the bound structure (Figure 2). In the ensemble of NMR constrained structure refinements, the K14 side chain rests in the phosphate backbone U-turn on the 5′ side of the loop with its ζ nitrogen 7.3 ± 1.2, 7.5 ± 1.0, and 7.5 ± 0.6 Å from the phosphates 5′ of C0 (the nucleotide directly 5′ of the GAAAA pentaloop), G1, and G2, respectively (*9*). The side chain of Q15 protrudes between the next two phosphates where the extruded nucleotide produces a bulge on the 3′ side of the loop. Its γ carbon is 4.1 ± 0.2 Å from the phosphate 5′ of A3 and 5.2 ± 0.1 Å from the next phosphate 5′ of A4. To a first approximation, we therefore expect cation replacement by K14 and volume exclusion by Q15 to account for the increased SK_{obs} of λ N (1−22) over λ N (1−11). The other

C-terminal charged K19 and E13 side chains are distant from the RNA backbone. Mutating K19 to alanine in λ N (1−22) does not appreciably alter its affinity, but substituting alanine for any of the other positively charged residues (including K14) decreases binding >50-fold (*15*). Since it has no role in affinity and is structurally shielded from the phosphate backbone by the peptide Q15 side chain and extruded RNA A4 base, we conclude that K19 has no effect on SK_{obs} for binding λ boxB. E13 faces directly away from the peptide−RNA interface, but it could slightly mitigate the salt dependence increase by restabilizing cations near K14.

The SK_{obs} values for R15 peptides are all at least as great as wild-type λ N (1−22) (Table 1). Ordering these peptides in terms of random region net charge or total number of positive charges does not reproduce the order of their salt dependencies. Structurally, sequence analysis and circular dichroism measurements of selected R15 peptides bound to λ boxB suggest that they all maintain the same bent α helical conformation as λ N up to at least position 16 (*19*). Accordingly, the side chains at positions 14 and 15 should occupy the same binding pockets near the phosphate backbone that they do in the λ N complex and largely determine the observed salt dependencies. This assumption proves powerful enough to rationalize all of the SK_{obs} values for R15 peptide binding to λ boxB. In selected peptides, the charge at these sites is reversed; R15 replaces Q15 and a nonbasic side chain substitutes for K14. The invariant R15 contributes a constant amount to SK_{obs} by cation replacement in all selected peptides. Its side chain guanidinium could interdigitate between the A3 and A4 phosphates in a forked conformation reminiscent of R8 and R11 in the λ N stem. The observation that mutating R15 to alanine causes the largest loss in binding affinity of any alanine mutation at positions 13−22 in peptide 11−36 supports this new electrostatic contact (*19*). The salt dependence of the peptides correlates with the negative polarity of the amino acid side chain at position 14 (in parentheses): 12−47 (E) ≈ 11−36 (E) < 12−39 (Q) < 11−10 (L) < 12−50 (M). These side chains generally cause an increase in salt dependence by sterically excluding cations from the volume near the phosphate backbone. Superimposed upon this effect is an opposite decrease in SK_{obs} from negatively charged or polar side chains restabilizing bound cations. This compensatory effect elegantly explains the observed functional covariation between positions 13 and 14 caused by an over-representation of ER pairs in selected peptide sequences (*19*). As was the case for λ N, other C-terminal side chains appear to have a negligible effect on the salt dependence of R15 peptide−λ boxB association.

Noncognate RNA Loop Binding. We were surprised to discover that the association constant for λ N (1−22) binding to the very similar GAAA and P22 boxB RNA loops has a significantly higher salt dependence than for binding its cognate λ boxB target (Table 1). In effect, its specificity against the noncognate loops increases at higher salt concentrations. λ N (1−22) discriminates against binding the GAAA tetraloop and P22 boxB by equilibrium constant factors of 4.5 and 30 in [M$^+$] = 50 mM salt but by 44 and 120 under higher [M$^+$] = 500 mM conditions. The R15 peptides 12−47 and 12−50 also have elevated salt dependencies for the other RNA loops in the same rank order as λ N (1−22): tetraloop > P22 boxB > λ boxB. In contrast, λ

N (1−11) and 11−36 have the same SK_{obs} for binding all three loops. What differs between these two classes of peptides? λ N (1−11) provides a constant stem that does not have different salt dependencies. By comparing peptides 12−47 and 11−36, we conclude that the elevated noncognate salt dependencies of 12−47 are a consequence of the two additional basic amino acid side chains (K17 and K20) near the C-terminus that are not involved in specific electrostatic interactions with λ boxB. 11−36 has no charged residues after the invariant E14 and R15 side chains and therefore has uniform SK_{obs} values. The observed graduated salt dependencies for λ N (1−22) and 12−50 binding are consistent with their nonspecific C-terminal K19 and R18 side chains.

All of these salt dependence effects are superimposed on overall differences in λ N and R15 peptide specificities (Figure 5). At reasonable salt concentrations (1 mM to 0.6 M), λ N (1−11) and λ N (1−22) discriminate much better against the P22 boxB hairpin than the GAAA tetraloop. We have previously noted that λ N (1−11) has the same specificity among these targets as λ N (1−22) (*18*). It follows that the C-terminal residues 12−22 of λ N must recognize shared features of all three loops to increase the overall affinity by about 3 orders of magnitude without changing the specificity. On the other hand, R15 peptides (11−36, 12−47, and 12−50) discriminate against the two noncognate loops equally and better than λ N does against the tetraloop. The increase in specificity against the tetraloop over the conserved λ N (1−11) stem implies that the C-terminal residues of R15 peptides recognize a shared loop feature of both P22 boxB and λ boxB that is not present in the tetraloop.

Structural Rearrangements Monitored by Fluorescence. We sought to understand the observed differences in specificity and salt dependence by comparing RNA and peptide structures in cognate and noncognate complexes. The structure of a bound RNA loop can be inferred from the change in 2AP fluorescence caused by peptide binding. The steady-state fluorescence intensity of 2AP in solution is quenched by aromatic base stacking and collisions with free nucleotides but is unaffected by base-pairing interactions (*28*). 2AP fluorescence changes in site-specifically labeled nucleic acids are commonly equated with differences in the extent of base stacking. This simplification is valid because the two quenching mechanisms are concerted in structured nucleic acids: local motions of adjacent stacked bases dominate the collisional quenching of 2AP in a double helix. Aromatic stacking on nucleotide bases will also quench the fluorescence of tryptophan and tyrosine amino acid side chains of the bound peptide.

GNRA tetraloops are known to rapidly equilibrate between multiple conformations with different loop stacking patterns when free in solution (*29, 30*), but only a single loop conformation is observed in NMR structures of GNRA-folded pentaloops bound to N peptides (*8, 10*). Therefore, the 2AP fluorescence changes induced in these RNA loops by peptide binding largely reflect the average change in the base stacking of a 2AP substituted nucleotide between an initial sampling of several stacked conformations and a constant final structure. The bound RNA could still be structurally degenerate in noncognate complexes, but peptide binding will perturb the relative energies of different stacked conformations such that the fluorescence changes.

Table 2: RNA Loop 2AP Fluorescence Changes Induced by Peptide Binding[a]

RNA Loop	λ boxB			tetraloop		P22 boxB	
	2AP−2	2AP−3	2AP−4	2AP−2	2AP−3	2AP−2	2AP−4
F_0	1.00 ± 0.03	1.95 ± 0.06	1.70 ± 0.05	1.55 ± 0.04	0.77 ± 0.02	0.66 ± 0.01	1.06 ± 0.03
Mg^{2+}	1.71 ± 0.06	0.61 ± 0.02	1.11 ± 0.05	1.42 ± 0.07	1.32 ± 0.02	0.65 ± 0.01	0.76 ± 0.06
λ N (1−22)	0.20 ± 0.03	0.19 ± 0.02	2.00 ± 0.06	0.06 ± 0.02	0.05	0.14 ± 0.04	2.77
λ N (1−11)	2.0 ± 0.1	−	−	1.67 ± 0.02	−	0.73 ± 0.03	−
11−10	1.94 ± 0.03	−	−	1.37	−	0.39	−
11−36	2.10 ± 0.03	0.20	2.13	1.84 ± 0.02	1.29	0.44 ± 0.03	2.27
12−39	2.12 ± 0.08	−	−	1.78	−	0.45	−
12−47	2.13 ± 0.08	−	−	1.84 ± 0.03	−	0.46 ± 0.02	−
12−50	2.12 ± 0.09	−	−	1.67 ± 0.06	−	0.47 ± 0.03	−

[a] F_0 is the fluorescence of an RNA relative to 2AP-2 λ boxB in the absence of any peptide. Mg^{2+} values are the total fluorescence change from fitting titrations to a two independent binding site model (Supporting Information). Peptide values are the fluorescence of the complex relative to the free RNA corrected to a monovalent concentration of 20 mM from the different [M⁺] present in different titrations as described in Materials and Methods. Errors are the standard deviations from four or more measurements at different [M⁺]. Values with no error indicated are from a single titration. A dash indicates that a value was not measured.

We supplemented the multiple titrations with 2AP-2 labeled loops used to construct the salt curves with single titrations using 2AP-3 and 2AP-4 labeled loops to more completely characterize bound RNA structures (Figure 4). We first titrated 2AP labeled loops with K⁺ and Mg^{2+} to observe the general effects of cations on loop structure (Supporting Information). K⁺ binding is nonspecific and could not be fit to a simple binding model. Mg^{2+} binding to all three RNA targets fits a two independent binding site model as was previously noted for the GAAA tetraloop (29).

Initial fluorescence intensities for all of the 2AP labeled RNA targets vary by only a factor of 3.0 (Table 2). This narrow fluorescence range is consistent with each loop initially equilibrating over an ensemble of different conformations to average the stacking of all loop bases. Metal or peptide binding should increase the fluorescence range roughly in proportion to the amount particular structures are individually stabilized relative to the rest of the initial ensemble. Accordingly, Mg^{2+}, 11−36, or λ N (1−22) binding increases the range to 5.1, 12.5, and 88.3, respectively.

λ N (1−22) binding quenches 2AP-2 and 2AP-3 λ boxB and enhances the fluorescence of 2AP-4 λ boxB. These changes agree with the known 4-out structure of the RNA loop in the cognate λ N-boxB complex. The A2 and A3 bases of the RNA loop are completely stacked under the peptide's W18 indole ring to form a GNRA tetraloop that excludes the destacked A4 base (8, 9). Noncognate binding of λ N (1−22) to the GAAA tetraloop also quenches 2AP-2 and 2AP-3 fluorescence. The first lab to solve the cognate NMR structure predicted that λ N could recognize a tetraloop with the same functional contacts (8). Our data agree with W18 forming a continuous stack with the A2 and A3 bases of the tetraloop analogous to the cognate complex. λ N (1−22) binding decreases the fluorescence of 2AP-2 P22 boxB and increases the fluorescence of 2AP-4 P22 boxB. These changes are not consistent with the bound RNA loop structure of the cognate P22 N-boxB complex (10). In this 3-out conformation, the A4 loop base would be stacked between A2 and A5 as part of the GNRA fold so its fluorescence should be quenched. The extruded C3 of the P22 boxB loop would also block W18 from stacking on A2. Yet, native tryptophan quenching in λ N (1−22) indicates that W18 is as stacked in this noncognate complex as it is in the cognate structure. Binding to λ boxB, the GAAA

tetraloop, and P22 boxB reduces W18 fluorescence to 0.13, 0.10, and 0.13 of its intensity in the free peptide, respectively. On the basis of the similarity of the P22 boxB and λ boxB fluorescence changes, we conclude that λ N (1−22) binding enforces the 4-out GNRA-folded pentaloop conformation of the P22 boxB RNA loop.

11−36 binding enhances the fluorescence of 2AP-2 and 2AP-4 λ boxB and quenches 2AP-3 λ boxB. The changes in 2AP-3 and 2AP-4 closely mirror those caused by λ N binding. We were uncertain what the 2AP-2 fluorescence change would be if the RNA loop adopted the same structure that it does in complex with λ N (1−22) without W18 stacking. Since λ N (1−11) recapitulates the specificity of the full peptide, it should be a reasonable proxy for the 2AP-2 fluorescence change induced by 4-out RNA loop folding without tryptophan stacking. λ N (1−11) binding enhances 2AP-2 fluorescence the same amount as 11−36, so we conclude that this R15 peptide also stabilizes the 4-out loop conformation of λ boxB. The fluorescence intensities of 2AP-2 and 2AP-3 GAAA tetraloops increase in response to 11−36 binding. This apparent decrease in stacking is similar to that observed for λ N (1−11) and Mg^{2+} binding. Without tryptophan enforcing full 3′ base stacking, polycation binding appears to stabilize less-stacked tetraloop conformations with more condensed phosphate backbones. 11−36 binding quenches the fluorescence of 2AP-2 P22 boxB and enhances 2AP-4 P22 boxB like λ N (1−22). Hence, it also imposes a GNRA-folded pentaloop conformation with the fourth base excluded on P22 boxB. It looks as if even λ N (1−11) binding slightly stabilizes the 4-out conformation from its slight quenching of 2AP-2 P22 boxB. Each selected peptide closely reproduces the fluorescence changes of 11−36 when binding the 2AP-2 labeled versions of all three RNA targets. We therefore believe that they all induce the same RNA loop structures because of the conserved R15 side chain. Minor deviations by 11−10 and 12−50 may be due to partial stacking by aromatic side chains.

Structural Rearrangements Monitored by CD. We used circular dichroism (CD) spectra to follow RNA and peptide conformational changes upon complex formation (Figure 6). It is difficult to identify specific RNA structural features in CD spectra, but it is easy to qualitatively compare conformational changes. To deconvolute portions of the spectra that are affected exclusively by RNA conformation from the superimposed RNA and peptide changes, we examined the
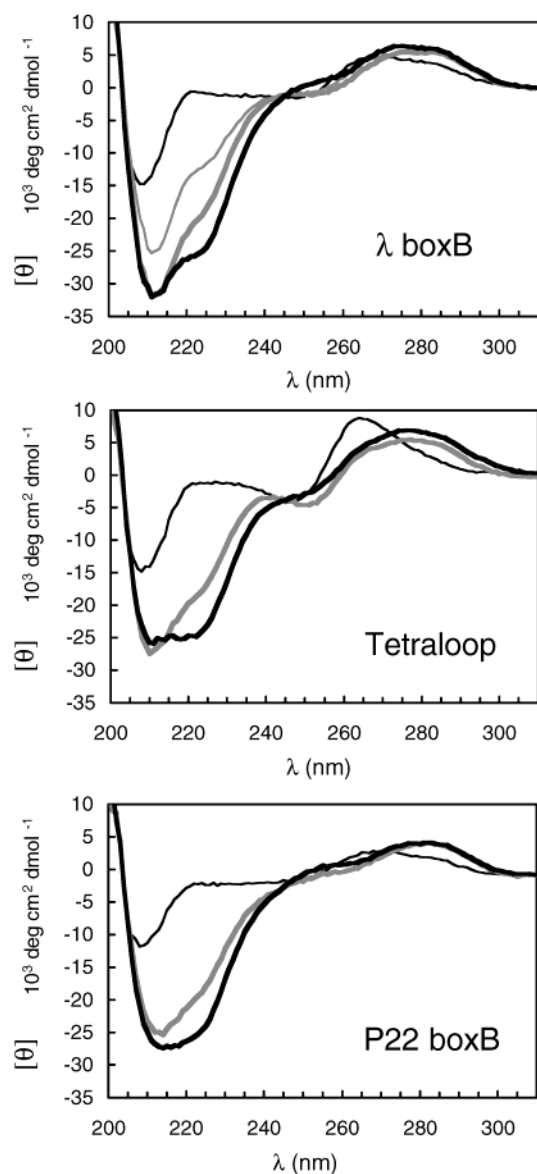
FIGURE 6: Difference circular dichroism spectra of Mg^{2+} and peptides bound to RNA targets. The thin black, thick black, thin gray, and thick gray lines represent Mg^{2+}, λ N (1−22), λ N (1−11), and λ N (11−36), respectively. Peptide complexes were stoichiometric, and 200 mM Mg^{2+} was chosen as a saturating amount of divalent metal. The molar ellipticities of the Mg^{2+} and λ N (1−11) complexes were normalized to the 22 residue length of the full peptides to allow direct comparisons of the induced RNA structure.

Table 3: Helicity of Bound Peptides[a]

	λ boxB		tetraloop		P22 boxB	
	$-[\theta]_{222}$	no. of AA	$-[\theta]_{222}$	no. of AA	$-[\theta]_{222}$	no. of AA
λ N (1−22)	25 800	16.0	24 800	15.4	25 600	15.9
λ N (1−11)	22 000	8.8	−	−	−	−
11−10	21 100	13.1	16 700	10.4	20 200	12.6
11−36	20 600	12.8	18 600	11.6	19 900	12.3
12−39	24 100	14.9	21 400	13.3	22 900	14.2
12−47	21 000	13.0	22 200	13.8	25 400	15.8
12−50	22 700	14.1	18 000	11.2	21 400	13.3

[a] $[\theta]_{222}$ is the molar residue ellipticity in deg cm^2 $dmol^{-1}$ from the complexed peptide difference spectra. We estimate a <5% error in the measurement of $[\theta]_{222}$. No. of AA is the number of helical amino acids calculated from $[\theta]_{222}$. There may be as high as a 15% error in no. of AA for λ N, 11−10, and 12−50 due to aromatic side chain contributions to $[\theta]_{222}$. A dash indicates that a value was not measured.

change reflects the same reorganization of the base-paired stem in all RNA−peptide complexes rather than a change in RNA loop conformation.

RNA−peptide complex CD spectra also reflect induced peptide structure. RNA binding induces specific α helical secondary structure in the initially unstructured wild-type λ N and selected R15 peptides. We previously used the ellipticity at 222 nm in the peptide−RNA complex difference spectra to calculate the effective number of helical amino acids in peptides bound to λ boxB (*19*). It is important to note that the 210 nm RNA peak does not appreciably affect determinations of peptide helicity using the ellipticity at 222 nm. Here, we have measured λ N and R15 peptide helicity in noncognate complexes with the GAAA tetraloop and P22 boxB (Table 3). For all peptides except 12−47 the magnitude of the induced helicity when bound to the three targets follows the same order: λ boxB > P22 boxB ≫ GAAA tetraloop. This consistent ranking might be caused by the same structural adjustments in the conserved N-terminal residues of every peptide. However, the range of differences between the helicity induced by λ boxB and tetraloop binding varies widely between 0.7 and 3.0 effective amino acids depending on the identity of the peptide. Additionally, helicity changes in the N-terminal moiety are unlikely because these residues almost exclusively contact the constant base-paired stem of the three RNA hairpins. We therefore believe that premature termination of peptide helices at the varying C-terminus causes the observed lower helicities in noncognate complexes.

DISCUSSION

On the basis of this information about the RNA and peptide conformations in noncognate complexes, we propose a structural model for λ N and R15 peptide specificity. Discrimination against binding the P22 boxB and GAAA loop sequences occurs by a combination of specific and nonspecific electrostatic recognition of the RNA phosphate backbone. Specific arginine contacts explain λ N (1−11) specificity and the greater discrimination of R15 peptides against the GAAA tetraloop. Nonspecific interactions with unstructured C-terminal basic residues in noncognate complexes are responsible for the higher salt dependencies of their association constants. For the purpose of presenting this model, we refer to RNA loops as if they existed in only a

effects of Mg^{2+} binding on free RNA targets. Mg^{2+} induces a narrow negative band centered at 210 nm and a wide positive peak around 260−270 nm. The former overlaps an induced peptide signal, so we use the second region from 250 to 310 nm as a fingerprint for induced RNA structure (*15*). The CD fingerprints of all three RNA targets bound to λ N (1−22) and 11−36 are very similar (Figure 6). 11−36 spectra are representative of all other R15 peptide complexes. Even λ N (1−11) induces the same changes as other peptides in λ boxB. As compared to the peptides, Mg^{2+} binding produces quite different CD fingerprints in RNA loops. The CD spectra of bound RNA loops corroborates the fluorescence data's conclusions that 11−36 and λ N both fold the pentaloops into the 4-out structure. However, we cannot entirely rule out the alternate possibility that the CD signal
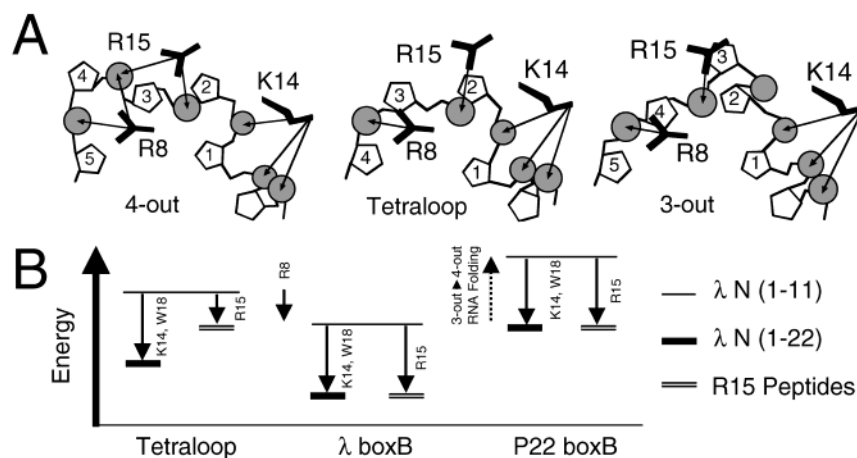
FIGURE 7: Peptide specificity model. (A) Locations of charged side chains relative to the phosphate-sugar backbone of the target loops. Phosphate groups are gray circles, and sugars are pentagons labeled by loop number. The λ N peptide-BoxB complex with the Q15R substitution was aligned with the other hairpins to construct this diagram. The λ boxB and P22 boxB structures in complex with their cognate peptides were used to represent 4-out and 3-out GNRA-folded pentaloops, respectively. (B) Hypothesized energetic consequences of different peptide side chain interactions and RNA conformational changes. λ N (1−11) binding reorganizes the P22 boxB loop to the less stable 4-out stacked structure. R8 interacts more favorably with the phosphate backbone of pentaloops than the GAAA tetraloop. λ N (1−22) has equally increased affinities for all three targets because its functional K14 and W19 side chains make identical contacts to the tetraloop and 4-out pentaloops. Selected peptides have increased specificity against the GAAA tetraloop because the conserved R15 preferentially recognizes the phosphate backbone of 4-out pentaloops.

few distinct, idealized conformations. As previously noted, both RNA loops and peptide C-terminal ends are likely to be flexible and structurally degenerate when they are not stabilized by any specific intermolecular contacts.

To understand what peptide side chains confer binding specificity and affinity, we modeled N peptides bound to a 3-out GNRA-folded pentaloop and the GAAA tetraloop and compared them to the 4-out GNRA-folded pentaloop structure. To do this, we replaced the GAAAA RNA pentaloop in the λ N-boxB complex with the RNA loops from the P22 N-boxB complex structure and the isolated GAAA tetraloop structure. This analysis reveals that some basic side chains of the λ N and R15 peptides preferentially contact the backbone phosphates of certain RNA loop conformations (Figure 7A). R8 and R15 are each within ∼5 Å of two loop phosphates when bound to the 4-out pentaloop, but they are only near one phosphate apiece in the tetraloop and 3-out pentaloop complexes. K14 and all other N-terminal arginines are near the same number of phosphates in all three conformations. On the basis of fluorescence changes in 2AP labeled loops and CD difference spectra, all of the peptides studied here bind the 4-out conformations of λ boxB and P22 boxB GNRA-folded pentaloops. The GAAAA λ boxB loop is more stable in this GNRA-folded conformation than the GACAA P22 boxB loop because it stacks a purine A3 versus a pyrimidine C3 between A2 and A5. Synthesizing the effects of RNA structural rearrangements and preferential side chain contacts gives a simple explanation for the surprising specificity of the N-terminal peptide fragment λ N (1−11) for λ boxB. Discrimination against the GAAA tetraloop is due to the loss of an R8 phosphate contact to its abbreviated phosphate backbone. λ N (1−11) makes the same functional contacts to P22 boxB as it does to λ boxB. However, binding the P22 boxB pentaloop is disfavored by the extra energy required to refold it into the 4-out conformation.

It is straightforward to explain the differences between λ N (1−22) and R15 peptide specificities by building on λ N

(1−11) discrimination. The price of refolding P22 boxB to the 4-out conformation has already been paid by λ N (1−11), so further increases in specificity are only possible by preferentially recognizing the 4-out pentaloop over the tetraloop. λ N (1−22) side chains contact these conformations equally. W18 can stack on the terminal RNA loop base in either structure, and K14 recognizes the invariant phosphate pocket on the 5′ side of the loop. Consequently, λ N (1−22) has the same specificity as λ N (1−11), although it has 100-fold increased affinity for all three targets. The distinguishing R15 side chain is responsible for the increased discrimination of selected peptides against the tetraloop. R15 is near two phosphates in the 4-out pentaloop as compared to just one in the tetraloop. Accordingly, the increase in affinity for both the λ boxB and P22 boxB pentaloops is about 10-fold greater than for the GAAA tetraloop. Figure 7B summarizes the energetics of noncognate RNA loop binding by λ N (1−11), λ N (1−22), and R15 peptides.

Our data implicate C-terminal basic side chains in nonspecific contacts to the RNA phosphate backbone that modulate N peptide binding specificity. The association of 11−36 and λ N (1−11) with all three RNA loops has the same salt dependence, but SK_{obs} values for λ N and R15 peptide binding to noncognate loops are elevated in the order λ boxB < P22 boxB < GAAA tetraloop. Interestingly, the amount of peptide helicity induced upon RNA binding varies between the loops so that GAAA tetraloop < P22 boxB < λ boxB for all but one peptide. Therefore, less bound peptide helicity corresponds to a higher salt dependence for peptides that have C-terminal positively charged side chains. This immediately suggests a model for the increased salt dependencies. Peptide unwinding in noncognate complexes allows charged side chains to explore further to find and nonspecifically bind RNA backbone phosphates. This limited unwinding can be compared to the extreme case of binding an unrelated RNA target. N peptides probably behave like model alanine-based peptides with spaced lysines when binding completely nonspecifically and partially collapse so

that every basic side chain localizes near the RNA phosphate backbone. Consequently, we expect that their bound helicities will converge to a low baseline, and salt dependencies will approach the theoretical maximum in this situation.

We are not sure why N peptides are less helical when bound to the P22 boxB and GAAA tetraloop targets. There may be two contributing explanations: (1) increased accessibility of RNA backbone phosphates could stabilize helix unwinding to interact with C-terminal basic side chains and (2) peptide side chains could specifically recognize the λ N loop structure to extend the helix. Structurally, both justifications seem plausible. Phosphates on the 3′ side of the loop that are blocked from the peptide-binding side by the excluded base in a 4-out GNRA-folded pentaloop are accessible in the GAAA tetraloop complex. On the other hand, the tetraloop lacks the excluded A4 of the λ boxB loop that could favorably contact the peptide to stabilize an extended α helix. P22 boxB appears to be intermediate between these two extremes. Its 4-out GNRA-folded pentaloop structure may not be identical to that of λ boxB because it forces the unfavorable submerged stacking of C3. The contributions of each effect to helix unwinding probably depend on the individual sequence of each peptide. We do know that loop recognition is involved in at least peptide 11−36 because it loses helicity in noncognate complexes and has no C-terminal charges. However, there is no correlation between the number of C-terminal charges or salt dependence and the loss of bound peptide helicity in noncognate complexes.

Typically, a nucleic acid binding protein is characterized by a specific affinity for its natural target and a nonspecific affinity for a completely unrelated binding site. It is important to also consider binding affinities for noncognate nucleic acid sites with similar sequences and structures—the very sites that the protein is likely to have the most trouble discriminating against. The models we present for N peptide recognition of GNRA-folded RNA loops are remarkable because they describe noncognate RNA−peptide complexes differing by only a single RNA loop nucleotide. The role of R15 in selected peptides best illustrates how the effect of a side chain can be different for noncognate and nonspecific binding. R15 increases discrimination against binding the noncognate GAAA tetraloop because it lacks a specific phosphate that is recognized in 4-out GNRA-folded pentaloops. On the other hand, the added positive charge of R15 in an unstructured peptide will generally decrease its discrimination against a nonspecific RNA target because it has electrostatic affinity for any polyanionic phosphate backbone. It is important for combinatorial and rational strategies to anticipate the added dimension of specificity against noncognate targets when designing macromolecular interactions (*31−33*). One can imagine how different the recognition spectra of proteins binding a specific DNA site would be if they were selected in the presence of a single DNA homopolymer as competitor or total cellular DNA and RNA.

REFERENCES

1. Weiss, M. A., and Narayana, N. (1998) *Biopolymers 48*, 167−180.
2. Puglisi, J. D., and Williamson, J. R. (1999) in *The RNA World* (Gesteland, R. F., Cech, T. R., and Atkins, J. F., Eds.) pp 405−425, Cold Spring Harbor Press, Woodbury, NY.
3. Ye, X. M., Gorin, A., Frederick, R., Hu, W. D., Majumdar, A., Xu, W. J., McLendon, G., Ellington, A., and Patel, D. J. (1999) *Chem. Biol. 6*, 657−669.
4. Heus, H. A., and Pardi, A. (1991) *Science 253*, 191−194.
5. Jucker, F. M., and Pardi, A. (1995) *RNA 1*, 219−222.
6. Jucker, F. M., Heus, H. A., Yip, P. F., Moors, E. H. M., and Pardi, A. (1996) *J. Mol. Biol. 264*, 968−980.
7. Abramovitz, D. L., and Pyle, A. M. (1997) *J. Mol. Biol. 266*, 493−506.
8. Legault, P., Li, J., Mogridge, J., Kay, L. E., and Greenblatt, J. (1998) *Cell 93*, 289−299.
9. Schärpf, M., Sticht, H., Schweimer, K., Boehm, M., Hoffmann, S., and Rösch, P. (2000) *Eur. J. Biochem. 267*, 2397−2408.
10. Cai, Z. P., Gorin, A., Frederick, R., Ye, X. M., Hu, W. D., Majumdar, A., Kettani, A., and Patel, D. J. (1998) *Nat. Struct. Biol. 5*, 203−212.
11. Doelling, J. H., and Franklin, N. C. (1989) *Nucleic Acids Res. 17*, 5565−5577.
12. Franklin, N. C. (1993) *J. Mol. Biol. 231*, 343−360.
13. Lazinski, D., Grzadzielska, E., and Das, A. (1989) *Cell 59*, 207−218.
14. Tan, R. Y., and Frankel, A. D. (1995) *Proc. Natl. Acad. Sci. U.S.A. 92*, 5282−5286.
15. Su, L., Radek, J. T., Hallenga, K., Hermanto, P., Chan, G., Labeots, L. A., and Weiss, M. A. (1997) *Biochemistry 36*, 12722−12732.
16. VanGilst, M. R., Rees, W. A., Das, A., and von Hippel, P. H. (1997) *Biochemistry 36*, 1514−1524.
17. Cilley, C. D., and Williamson, J. R. (1997) *RNA 3*, 57−67.
18. Barrick, J. E., Takahashi, T. T., Ren, J. S., Xia, T. B., and Roberts, R. W. (2001) *Proc. Natl. Acad. Sci. U.S.A. 98*, 12374−12378.
19. Barrick, J. E., and Roberts, R. W. (2002) *Protein Sci. 11*, 2688−2696.
20. Guex, N., and Peitsch, M. C. (1997) *Electrophoresis 18*, 2714−2723.
21. Record, M. T., Anderson, C. F., and Lohman, T. M. (1978) *Q. Rev. Biophys. 11*, 103−178.
22. Mascotti, D. P., and Lohman, T. M. (1997) *Biochemistry 36*, 7272−7279.
23. Mascotti, D. P., and Lohman, T. M. (1992) *Biochemistry 31*, 8932−8946.
24. Padmanabhan, S., Zhang, W. T., Capp, M. W., Anderson, C. F., and Record, M. T. (1997) *Biochemistry 36*, 5193−5206.
25. GuhaThakurta, D., and Draper, D. E. (2000) *J. Mol. Biol. 295*, 569−580.
26. Misra, V. K., Hecht, J. L., Sharp, K. A., Friedman, R. A., and Honig, B. (1994) *J. Mol. Biol. 238*, 264−280.
27. Jayaram, B., Dicapua, F. M., and Beveridge, D. L. (1991) *J. Am. Chem. Soc. 113*, 5211−5215.
28. Rachofsky, E. L., Osman, R., and Ross, J. B. A. (2001) *Biochemistry 40*, 946−956.
29. Menger, M., Eckstein, F., and Porschke, D. (2000) *Biochemistry 39*, 4500−4507.
30. Sorin, E. J., Engelhardt, M. A., Herschlag, D., and Pande, V. S. (2002) *J. Mol. Biol. 317*, 493−506.
31. Jenison, R. D., Gill, S. C., Pardi, A., and Polisky, B. (1994) *Science 263*, 1425−1429.
32. Wallace, S. T., and Schroeder, R. (1998) *RNA 4*, 112−123.
33. Hirao, I., Spingola, M., Peabody, D., and Ellington, A. D. (1998) *Mol. Diversity 4*, 75−89.